RESEARCH PAPER

Synthesis and Characterization of $LiMn_2O_4$ as a Cathode Material for Lithium-Ion Batteries

Noor M. Ali [1], O. A. Al-Jubouri [2], M.H. Al-Al-Timimi [2], H.T. Homad [2]*

[1] *Department of Physics; College of Science; Diyala University, Diyala, Iraq*

[2] *Physics Department, College of science, Diyala University, Diyala, Iraq*

ARTICLE INFO

Article History:
Received 27 January 2025
Accepted 22 March 2025
Published 01 April 2025

Keywords:
CV
EIS
Sol-gel method
Warburg Impedance

ABSTRACT

In this study, the spinel compound $LiMn_2O_4$ was manufactured as the cathode active material for Li-ion batteries via the sol–gel process. The field-emission scanning electron microscope (FESEM) was employed for an evaluative analysis of the external surface morphology of the synthesized material. The crystal structure of the spinel material was confirmed using X-ray diffractometry (XRD). The XRD graph exhibited no signs of impurity peaks, confirming a singular crystal structure phase. As per the Scherrer equation, the crystal size was estimated at 31.98 nm. The energy-dispersive X-ray spectroscopy (EDX) spectra for the equipped sample showed the existence of manganese and oxygen, and the concentrations were very close to the elemental composition used. Electrochemical attributes were investigated through galvanostatic charge–discharge (GCD) cycling and cyclic voltammetry (CV) in a voltage range of 2.5 to 4.8 V. The $LiMn_2O_4$sample displayed a charge capacity of 116.5 $mAhg^{-1}$ and a discharge capacity of 114.3 $mAhg^{-1}$. The Coulombic efficiency exhibited by this electrode was 98.1%. After 100 cycles, the capacity retention was as high as 75.8%. The electrochemical impedance spectroscopy (EIS) measurements of the $LiMn_2O_4$ electrode, including the electrolyte bulk resistance (R_s), charge transfer resistance (R_{ct}), and Warburg Impedance (W_o), were 13.3 ohms, 118.7 ohms, and 0.61 ohms, respectively.

How to cite this article
Ali N., Al-Jubouri O., Al-Al-Timimi M., Homad H. Synthesis and Characterization of $LiMn_2O_4$ as a Cathode Material for Lithium-Ion Batteries. J Nanostruct, 2025; 15(2):702-711. DOI: 10.22052/JNS.2025.02.028

INTRODUCTION

Researchers continuously explore and optimize preparation methods to tailor materials for specific battery applications, considering these factors to achieve improved electrochemical properties. The goal is to develop materials that offer higher energy density, longer cycle life, and better overall performance in diverse battery technologies. Because of their high voltage, large capacity, and extended cycle life, Li-ion batteries are frequently employed in electronic devices like cell phones As well as portable recording devices [1]. Because of its abundance in manganese, low cost, and lower toxicity, spinel lithium manganese oxide has gained considerable interest as the most optimistic cathode material for Li secondary batteries [2]. However, when compared to layered compounds, $LiMn_2O_4$ falls short [3] Because of capacity fading within the 4.0 volt range. Researchers have explored solutions to these issues, including

* *Corresponding Author Email: nmask88@gmail.com*

the examination of non-stoichiometric lithium manganese spinels, modification of the surface through coating with oxide or carbon, and partial replacement of manganese ions with foreign ions [4]. The electro-chemical parameters of electrode materials are generally influenced by chemical and physical characteristics including crystallite size, homogeneity, and stoichiometry [5]. Achieving the required capacity for the cell necessitates a small and consistent particle size. Surface morphology and particle size are associated with charge-discharge rate capabilities [6], safety, and cell efficiency. Particularly, small particle size improves the cycle ability and rate capability of the cathode material [7]. Understanding and optimizing the preparation method are essential steps in tailoring materials for specific electrochemical applications, ensuring that the resulting materials exhibit desirable properties for use in batteries, supercapacitors, fuel cells, or other devices. Researchers often explore different synthesis routes to identify the most effective method for enhancing electrochemical performance. Various synthesis techniques for $LiMn_2O_4$ thin films have been reported by many groups, including the hydrothermal technique, sol-gel method [8,9], electrostatic spray deposition [10], radio frequency magnetron sputtering [11], and pulse laser deposition [12].

In this current investigation, we prepared and analyzed the structural and morphological characteristics of the cathode's active material designed for lithium-ion batteries, employing both the sol-gel and hydrothermal techniques. The primary objective is to clarify the electrochemical attributes of each cathode and determine the more effective method between the two for creating a cathode with unique electrochemical properties.

MATERIALS AND METHODS

Synthesis of $LiMn_2O_4$ nanoparticles

Nanoparticles of ($LiMn_2O_4$) were synthesized via the sol-gel process. Precise amounts of LiCl (lithium chloride) (THOMAS Baker), $MnCl_2.4H_2O$ (manganese chloride tetrahydrate) (Alpha Chemical), and citric acid ($C_6H_8O_7$) (THOMAS Baker) had weighed based on their molecular weights. These materials were combined in a glass beaker and thoroughly mixed at ~27 using a high-speed magnetic mixer until a smooth and slimy red solution was obtained. Ammonium hydroxide (NH_4OH)(ROMIL Pure Chemistry) solution was then added gradually, drop by drop, to the combined solution to adjust its pH scale to the desired range of (6.9 to 7), while continuous stirring was maintained. This resulted in a dark brown solution. The heat of the solution was gradually elevated to 60°C for one hour and then further increased to 90°C. Over the course of approximately 30 minutes, the solution's viscosity increased significantly, leading to the formation of gel, primarily in the middle of the solution. Eventually, the entire solution transformed into a gel state, even while still under magnetic stirring at a heat of 90°C.Once the gel formation was complete, the temperature was lowered back to room temperature. The gel was allowed to dry, resulting in a dark brown color. The drying process was conducted within an oven at 70°C for duration of 4 hours to ensure the removal of all residual distilled water. Subsequently, the gel was subjected to calcination in an air environment at 800°C for a total of 4 hours. The Supplier Companies and Model for XRD, FESEM, EDS, CV, EIS, and GCD were XRD 6000-Shimadzu/Japan, MIRA3-TESCAN, Screenshot showing 3D Tomography module-Tescan VegaIII-Czech Republic/USA, model CT-3008, model WisEIS-8100 premium, and workstation (CHI660E).

RESULTS AND DISCUSSION

X-ray Diffraction Analysis

X-ray test are conducted on the sample included that were equipped by the sol-gel. Fig. 1 illustrates the XRD pattern of sample prepared. It was noticed formation of single-phase $LiMn_2O_4$. XRD data of the sample well matched with the Joint Committee on Powder Diffraction Standards (JCPDS).

A detailed evaluation of all cell parameters had been undertaken for XRD analysis on the chemical $LiMn_2O_4$. The sample reveal single-phase cubic spinel with the Fd-3m space group and favorable orientations of six characteristic peaks: (111), (311), (222), (400), (331), and (511). They are cataloged with JCPDs card no. 35-0782. This means the spinel $LiMn_2O_4$ has been prepared successfully using the sol-gel technique in addition to no phase impurities were detected (absence of impurity phases). In the spinel $LiMn_2O_4$ structure, the tetrahedral positions (8a) are filled by lithium, the octahedral sites (16d) are occupied by manganese, and the (32e) sites host the oxygen

ions, as documented in references [13,14].The sample were revealed by their strong and sharp reflections to be well crystallized. Depending on the X-ray diffraction results, these samples had been chosen in this study and calculate the lattice constant (a_{exp}), X-Ray density, Crystallite Size (D), in addition to Hopping length (Å). The peak broadening validates the presence of nanosized particles. The experimental lattice parameter (a_{exp}) was determined by the following relation [15]:

$$a_{exp} = d\sqrt{h^2 + k^2 + l^2} \quad (1)$$

Where each plane's interplanar distance is represented by d, as well as (hkl) corresponds to Miller indices, D_{ave} computed the average crystallite size using the established Scherrer equation:

$$D_{ave} = K\lambda/\beta \cos\theta \quad (2)$$

Dave represents the average size of crystallites, with K symbolizing the Scherrer constant ($K = 94\times10^{-2}$), where λ stands for the wavelength of the employed X-ray, β denotes the full width at half maximum, and θ represents the Bragg angle. The volume of the unit cell in its cubic structure is determined using equation (3), and equation (4) is utilized to calculate the X-ray density (ρ_x) based on XRD data.

$$V_c = a_{exp}^3 \quad (3)$$

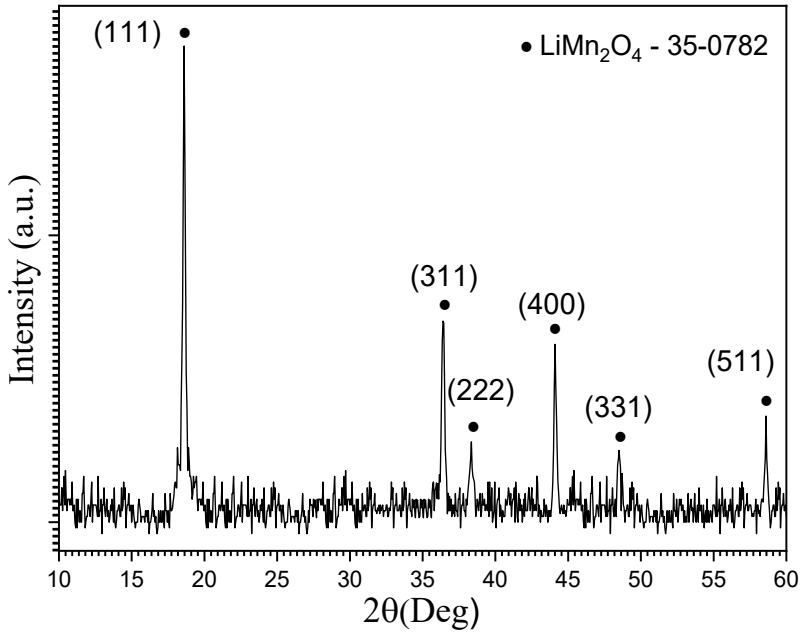

Fig. 1. XRD results of the $LiMn_2O_4$ samples.

Table 1. XRD Calculation of $LiMn_2O_4$ Nanoparticles.

Lattice constant		Molecular mass	X-ray density	crystallite size (D_{111})	Hopping length (Å)		
a_{exp} (Å)	V (Å)	g.mol^{-1}	ρ_x (g/cm^3)	D_{ave} (nm)	L_{A-A}	L_{B-B}	L_{A-B}
8.2501	561.5360	180.814	4.277	31.98	3.5723	2.9168	3.4203

$$\rho_x = \frac{Z\,M}{N_A\,V_c} \quad (4)$$

Z corresponds to the count of formula units within a unit cell (Z = 8 for the spinel system), where M signifies the molecular weight of the sample, N_A stands for Avogadro's number, in addition to V_c denotes the cell's volume [15].

The distances for hopping, namely $L_{A\text{-}A}$, $L_{B\text{-}B}$, in addition $L_{A\text{-}B}$, between ions situated at the A-site and B-site, were evaluated using the expressions:

$$L_{A-A} = (a_{exp}\sqrt{3})/4 \quad (5)$$

$$L_{B-B} = (a_{exp}\sqrt{2})/4 \quad (6)$$

$$L_{A-B} = (a_{exp}\sqrt{11})/8 \quad (7)$$

$L_{A\text{-}A}$, $L_{B\text{-}B}$, plus $L_{A\text{-}B}$ denote the distances corresponding to Tetra-tetra A-A, Octa-octa B-B, plus Tetra-octa A-B, respectively [16]. Table 1 presents the XRD calculations of the (111) phase for $LiMn_2O_4$ sample.

FESEM image analysis of $LiMn_2O_4$

The morphology of the prepared materials was explored through the application of Field Emission Scanning Electron Microscopy (FESEM), as illustrated in the Fig. 2. The materials were prepared in one manner and subjected to FESEM examination. The resulting images were interpreted as follows. The images produced using sol-gel method in this study a certain resembles those acquired by earlier researchers who produced the same materials. Nevertheless, noteworthy differences were noted, potentially stemming from variances in preparation method, processing temperatures, types of raw materials, and other contributing factors.

FESEM images of $LiMn_2O_4$ compound reveal that most particles obtained via the sol-gel method employing citric acid exhibit a geometric form known as an octahedron (octahedral or octahedrons). An octahedron is a three-dimensional polyhedron with eight faces, twelve sides, and six vertices. Additionally, there is the presence of crystalline octahedral particles, characterized by a smooth and clean surface with diameters ranging from several tens to hundreds of nanometers. These particles demonstrate a higher degree of dispersion, and the bridging phenomenon is not apparent, indicating that the particles are separated from one another. The substantial dispersion of particles is advantageous for facilitating contact with the electrolyte, thereby improving high-rate capability.

Energy Dispersive X-Ray Spectroscopy

The elemental composition of the ready

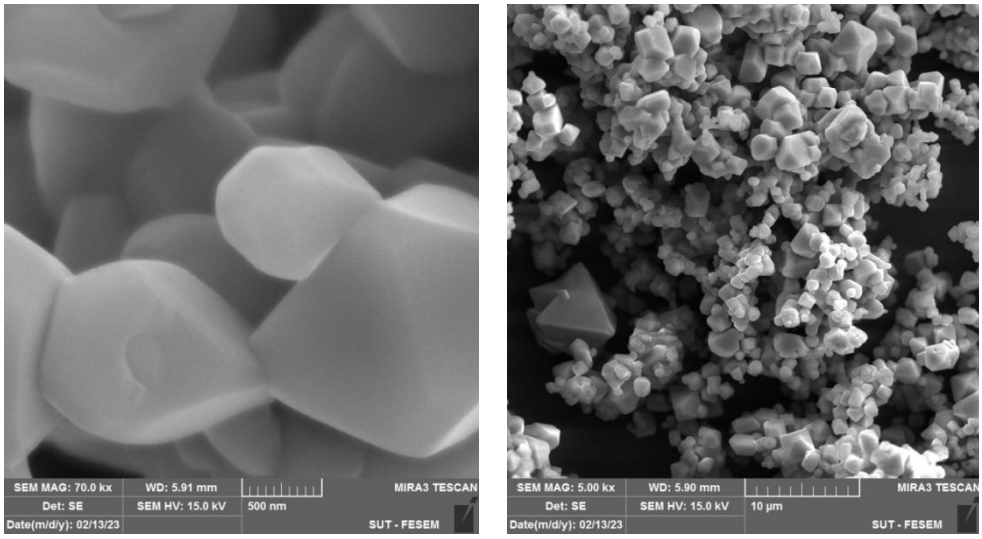

Fig. 2. FESEM images and particle distribution of $LiMn_2O_4$ powder.

material was analyzed utilizing the EDX technique within the 0 - 10 keV range. The EDX spectra (Fig. 3) of the equipped sample reveal the existence of Manganese and Oxygen, with concentrations closely matching the specified elemental composition. Additionally, no impurity peaks were observed in the EDS pattern. It's important to highlight that the detectors in the EDX device are calibrated to recognize radiations of specific energy; any energy below the calibrated value is undetectable by the detectors. Since X-rays produced by Li elements have very little energy, their detection is not possible with the radiation detector [17].

Several factors contribute to the difficulties in detecting lithium with EDX include lithium has a low atomic number (Z=3). Elements with low atomic numbers generally produce weak X-ray signals. The intensity of characteristic X-rays emitted during the interaction of the incident X-ray beam with lithium atoms is inherently low, making it difficult to distinguish the signal from the background noise. Moreover, the X-ray emission efficiency of lithium is relatively low compared to heavier elements. This means that the emitted X-rays from lithium are weak, further complicating their detection. Additionlity, lithium X-rays are susceptible to absorption and scattering effects within the sample matrix. These phenomena lead to a reduction in the intensity of the emitted X-rays, affecting the signal-to-noise ratio and making it challenging to accurately identify and quantify lithium. Besides, the sensitivity of EDX is influenced by the instrument's design and specifications. Many EDX systems are optimized for detecting mid to high atomic number

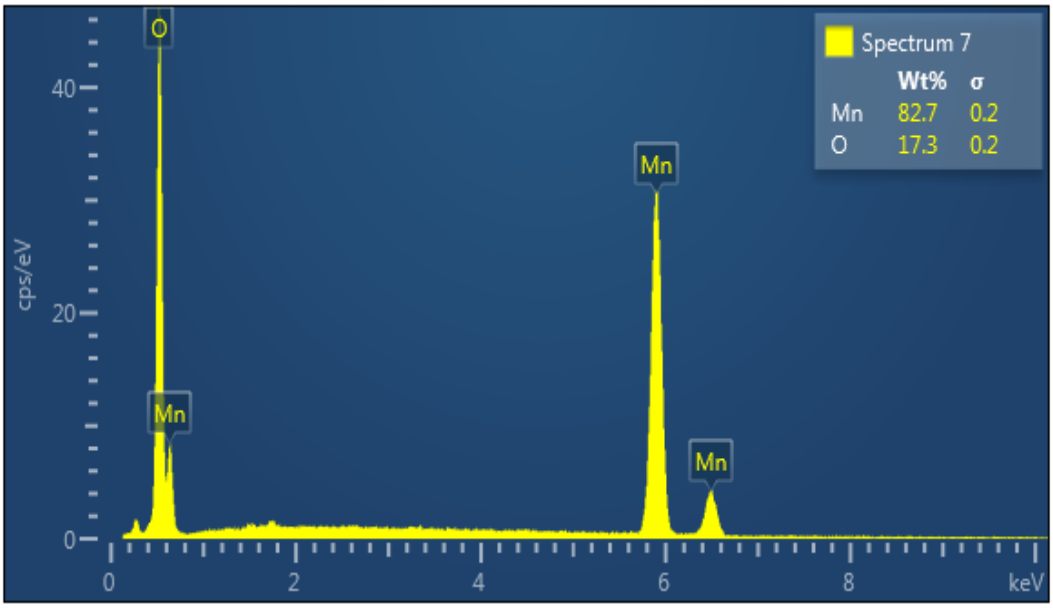

Fig. 3. EDS analysis of $LiMn_2O_4$.

Table 2. EDS analysis of $LiMn_2O_4$ sample.

Element	Line Type	Weight %	Atomic %
O	K series	17.30	41.81
Mn	K series	82.70	58.19
Total:		100.00	100.00

elements, and their performance may be limited for light elements like lithium, especially when present in trace amounts. The X-ray peaks from lithium may overlap with other nearby peaks in the spectrum, particularly in complex samples. This overlap complicates the deconvolution of signals and introduces challenges in the accurate identification of lithium. Also, the form in which lithium is present in the sample can impact its detectability. If lithium is unevenly distributed or present in very small amounts, it may not produce a discernible signal. Additionally, certain sample preparation techniques may influence the visibility of light elements in EDX analysis [18, 19].

Electrochemical properties of $LiMn_2O_4$

Fig. 4 demonstrates the cyclic voltammetry (CV) diagrams of the $LiMn_2O_4$ cathode synthesized by the sol gel technique. The CV measurement was carried out in the potential range of 2.5 to 4.8 V. Cyclic voltammetry is a powerful and broad appealing electrochemical means typically adopted to meticulously study the reduction and oxidation processes of molecular species in lithium-ion batteries. CV is also a beneficial technique to investigate the electron transfer-initiated chemical reactions in these energy storage devices [20].

According to (Fig. 4), two distinct and well-defined pairs of the redox peaks are observed for the $LiMn_2O_4$ cathode fabricated via the sol-gel technique. Both peaks are attributed to the intercalation/de-intercalation of the Li ions to or from the cathode material, a cathodic peak of 4.0815/4.2269 V and anodic peaks of 4.1246/4.2686 V can be observed for this sample. The change in the intensity of the redox peaks and also their location with scan rate can be a good parameter to study the kinetics of lithium ion battery intercalation and de-intercalation process.

Several important factors that influenced the electrochemical performance, both positively and negatively, must be mentioned. The cyclic voltammetry exhibited two sets of distinct reversible redox peaks, characteristic of a stoichiometric spinel phase. These two-step processes are related with the ordering of Li ions on half of the tetrahedral 8a positions, as described in the literature, leading to Mn^{3+}/Mn^{4+} redox reactions [21]. Another piece of evidence suggesting minute Mn dissolution is that the reduction current peaks recorded almost the same values as the oxidation current peaks. The samples with the highest peak current and peak area exhibit a higher discharge capacity than the other samples. Additionally, samples with an anodic peak shift toward lower voltage and a cathodic peak shift toward higher voltage exhibit higher kinetics of lithium-ion diffusion [22]. The good structural arrangement, confirmed by the FESEM study and the higher surface area and shorter particle size, leads to an

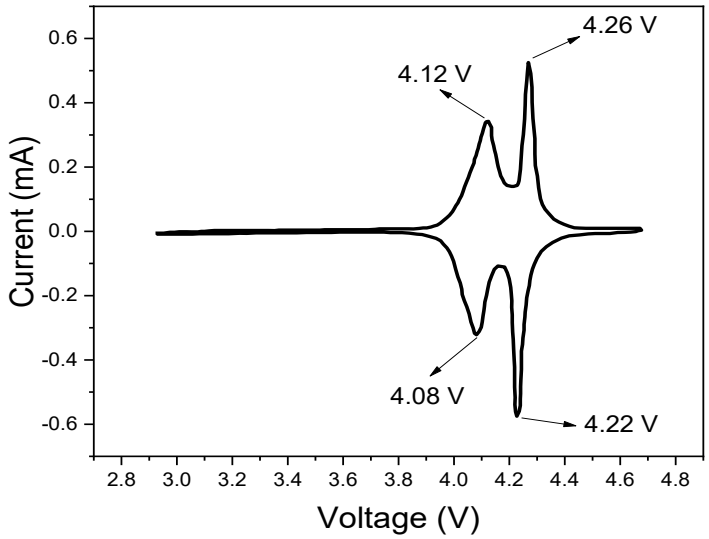

Fig. 4. The CV for $LiMn_2O_4$ was obtained at a scanning rate of 1 mV/s within the voltage range of 2.0 to 4.8 volts.

increase in electrochemical activity. However, the formation of a secondary phase at specific doping concentrations weakens the bonds in materials prepared in octahedrons, leading to a decrease in electrochemical activity. Samples with sharper and more symmetrical redox peaks demonstrate a higher rate of lithium-ion intercalation and deintercalation. Also, their smaller difference between redox potential and minimal electrode polarization during the charging/discharging

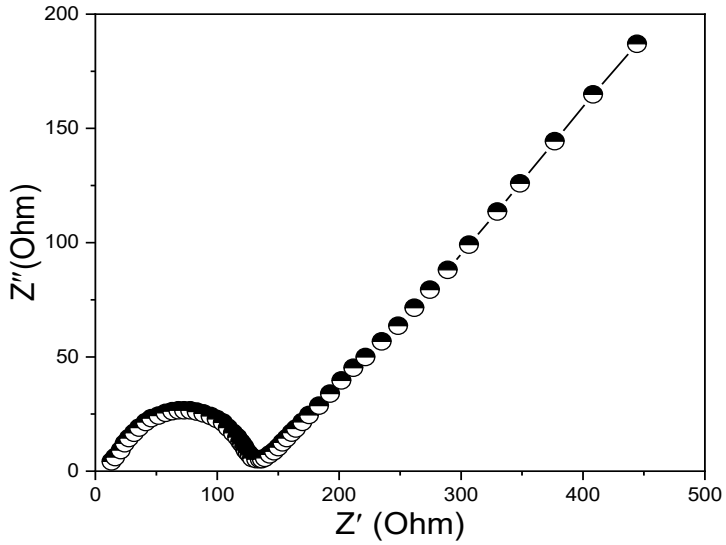

Fig. 5. The Nyquist plot of the $LiMn_2O_4$ cathodes.

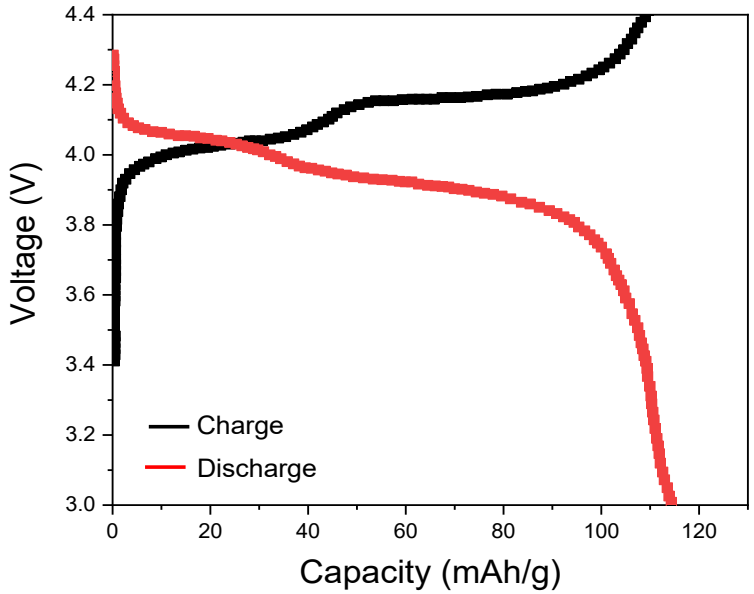

Fig. 6. The initial charge/discharge cycle of the half cells composed of lithium counter electrode and $LiMn_2O_4$ as the working electrode recorded in the voltage of 2.0 to 4.8 V and the C-rate of 0.1.

process contributes to good cyclic performance [23-25].

Referring to the EIS test is essential, as it holds great importance and provides a comprehensive understanding of electrochemical properties. The principle of the EIS is application of a perturbation to an electro-chemical system in equilibrium or in steady state by using a sinusoidal signal (alternative current (AC) voltage or AC current) within a broad range of frequencies and recording the sinusoidal responses (current or voltage, respectively) of the system toward the applied perturbation. It should be considered that the system under study is a linear time-invariant electrochemical system where the output signal has a linear relationship with the input signal as well as no change in the system's behavior is observed over time. EIS is a transfer function method modeling the output signal (AC current or AC voltage) to the input signal (AC voltage or AC current) within a broad range of frequencies [26].

The Nyquist plots of the cathodes in LIBs are commonly made up of a semicircle at medium-to-low frequency accompanied by a straight slope line located at low frequency. The intersection point of the curves and the Z_{re} axis at high frequency is imputed to the electrolyte's ionic conductivity (electrolyte bulk resistance or R_s). The semicircular varying from the medium to low frequency is ascribed to the charge transfer resistance between the electrode/electrolyte and also the kinetic of the electrochemical reactions occurred in electrode (R_{ct}). The straight slope line known as the Warburg impedance (W_o) is relevant to the diffusion of lithium ions within the bulk of the host compound [27]. To elaborate further, a straight line in the plot indicates the diffusion or intercalation/de-intercalation manner of lithium ions. The existence of a straight line suggests that Li ions can transfer simply from the cathode through the electrolyte and couple with electrons on the anode. A steeper, more upright straight line signifies a faster diffusion path [28].

The EIS measurements of the $LiMn_2O_4$ electrode include the electrolyte bulk resistance or R_s, charge transfer resistance (R_{ct}), and Warburg Impedance (W_o). The values for R_s, R_{ct}, and W_o are 13.3 ohms, 118.7 ohms, and 0.61 ohms, respectively (Fig. 5). The previous EIS parameters for the $LiMn_2O_4$ electrode indicate good diffusion of lithium ions within the electrode structure. These results align with the cyclic voltammetry (CV) data, where the $LiMn_2O_4$ electrode exhibited redox peaks. Furthermore, the distance between the

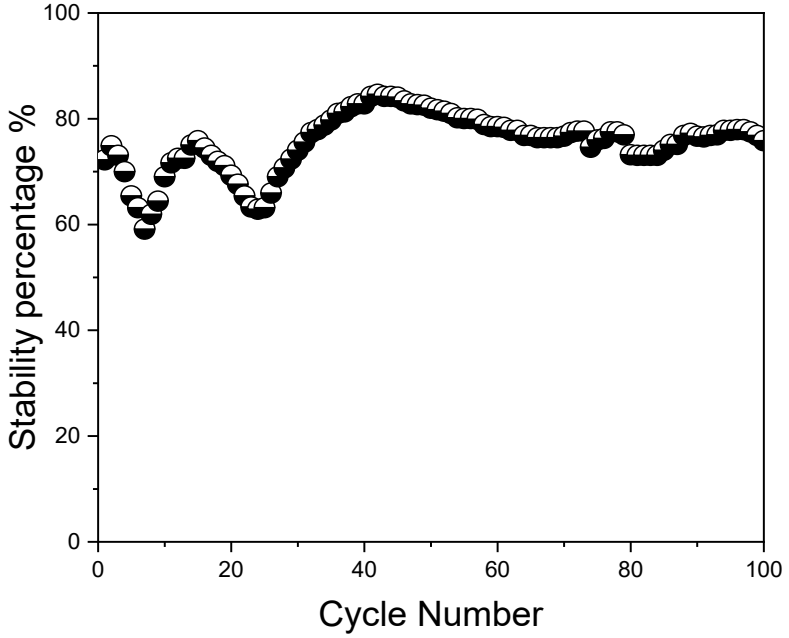

Fig. 7. The stability percentage versus the cycle number of the $LiMn_2O_4$ cathode materials after 100 cycles in the voltage varying from 2.0 to 4.8 V and the C-rate of 0.1.

pair of redox peaks was lower for this electrode, attributed to reduced polarization in the $LiMn_2O_4$ electrode.

Due to its significance in assessing battery performance, reference was also made to the charging and discharging processes. The $LiMn_2O_4$cathode (in Fig. 6), fabricated through the sol-gel process, displayed a charge capacity of 116.5 $mAh.g^{-1}$ and a discharge capacity of 114.3 $mAh.g^{-1}$. Additionally, the Coulombic efficiency exhibited by this electrode was 98.1%. The Coulombic efficiency of a battery is a crucial metric in evaluating its performance over charge and discharge cycles. Coulombic efficiency is typically expressed as a percentage and is calculated by comparing the amount of charge delivered during discharge to the amount of charge supplied during charging. It is important to note that achieving a high Coulombic efficiency indicates minimal capacity fade between discharge and charge cycles. The superior electrochemical performance of the sol-gel-based $LiMn_2O_4$ cathode can be attributed to the adoption of this method, which resulted in a cathode material with a structure that facilitates the transportation of lithium ions and enhances the movement of charges within the electrode. This improvement in lithium ion diffusion is supported by both cyclic voltammetry (CV) and electrochemical impedance spectroscopy (EIS) measurements.

Finally, the measurements were carried out using half-cells consisting of the lithium as the counter electrode and $LiMn_2O_4$ cathode material as the working electrode. The cycling performance of the electrodes was evaluated using a Neware multi-channel battery tester. The cycle life of a battery can be defined as the number of charging and discharging cycles that a battery can achieve before its capacity is completely depleted. A Li-ion battery with high performance should able to keep its capacity constant even after several charging and discharging cycles. The cycle life of Li ion batteries immensely relies on the structural stability of the active materials of the electrode during the charge and discharging process.

The one produced by the sol-gel technique delivered higher capacity retention after 100 cycles. Accordingly, the $LiMn_2O_4$ electrode showed capacity retention of 75.8% (Fig. 7). As evidenced by these analyses, the $LiMn_2O_4$ electrode showed low in polarization and charge transfer resistance, which can be attributed to its good structure to easily transport the lithium ions within the electrode. The rapid movement of lithium ions within the fabricated electrode resulted in decreased polarization and improved conductivity.

CONCLUSION

The sol-gel method was employed to effectively manufacture $LiMn_2O_4$ for use as a cathode in lithium-ion batteries. Structural and morphological tests have shown that it is possible to produce these materials with spinel structures characterized by high crystallinity and well-defined compositions. The electrochemical performance of these materials was examined through various analyses, including cyclic voltammetry, electrochemical impedance spectroscopy, initial charge/discharge cycles, and capacity retention measurements. The method used to prepare electrode materials significantly influences the structure, morphology, and surface characteristics of the particles. Consequently, these factors can lead to materials with improved conductivity, enhanced structural stability, and a favorable electrode-electrolyte interface. This, in turn, contributes to better charge retention over the battery's lifetime.

ACKNOWLEDGMENTS

The authors express their gratitude to the University of Diyala, College of Science, Department of Physics, for furnishing the necessary tools, materials, and support for this paper.

CONFLICT OF INTEREST

The authors declare that there is no conflict of interests regarding the publication of this manuscript.

REFERENCES

1. Goodenough JB, Kim Y. Challenges for Rechargeable Li Batteries. Chem Mater. 2009;22(3):587-603.
2. Luo J-Y, Li X-L, Xia Y-Y. Synthesis of highly crystalline spinel $LiMn_2O_4$ by a soft chemical route and its electrochemical performance. Electrochimica Acta. 2007;52(13):4525-4531.
3. Myung S-T, Chung H-T, Komaba S, Kumagai N, Gu H-B. Capacity fading of $LiMn_2O_4$ electrode synthesized by the emulsion drying method. J Power Sources. 2000;90(1):103-108.
4. Michalska M, Lipińska L, Mirkowska M, Aksienionek M, Diduszko R, Wasiucionek M. Nanocrystalline lithium–manganese oxide spinels for Li-ion batteries — Sol-gel synthesis and characterization of their structure and selected physical properties. Solid State Ionics. 2011;188(1):160-164.
5. Suryakala K, Marikkannu KR, Kalaignan GP, Vasudevan T. Synthesis and Electrochemical Characterization of

$LiMn_2O_4$ and LiNd Mn1.7O4 as Cathode for Lithium Ion Battery. International Journal of Electrochemical Science. 2008;3(2):136-144.
6. Qiao Y, Li S-R, Yu Y, Chen C-H. Synthesis and electrochemical properties of high performance yolk-structured $LiMn_2O_4$ microspheres for lithium ion batteries. J Mater Chem A. 2013;1(3):860-867.
7. Goriparti S, Miele E, De Angelis F, Di Fabrizio E, Proietti Zaccaria R, Capiglia C. Review on recent progress of nanostructured anode materials for Li-ion batteries. J Power Sources. 2014;257:421-443.
8. Park YJ, Kim JG, Kim MK, Chung HT, Um WS, Kim MH, et al. Fabrication of LiMn2O4 thin films by sol–gel method for cathode materials of microbattery. J Power Sources. 1998;76(1):41-47.
9. Park Y. Preparation of $LiMn_2O_4$ thin films by a sol–gel method. Solid State Ionics. 2000;130(3-4):203-214.
10. Anzue N, Itoh T, Mohamedi M, Umeda M, Uchida I. In situ Raman spectroscopic study of thin-film Li1−Mn2O4 electrodes. Solid State Ionics. 2003;156(3-4):301-307.
11. Komaba S, Kumagai N, Baba M, Miura F, Fujita N, Groult H, et al. Preparation of Li–Mn–O thin films by r.f.-sputtering method and its application to rechargeable batteries. J Appl Electrochem. 2000;30(10):1179-1182.
12. Sonoyama N, Iwase K, Takatsuka H, Matsumura T, Imanishi N, Takeda Y, et al. Electrochemistry of LiMn2O4 epitaxial films deposited on various single crystal substrates. J Power Sources. 2009;189(1):561-565.
13. Guo H-j, Li X-q, He F-y, Li X-h, Wang Z-x, Peng W-j. Effects of sodium substitution on properties of LiMn2O4 cathode for lithium ion batteries. Transactions of Nonferrous Metals Society of China. 2010;20(6):1043-1048.
14. Chen Y-C, Xie K, Pan Y, Zheng C-M, Wang H-L. High power nano-$LiMn_2O_4$ cathode materials with high-rate pulse discharge capability for lithium-ion batteries. Chinese Physics B. 2011;20(2):028201.
15. An Organic/Inorganic Nanocomposite of Cellulose Nanofibers and ZnO Nanorods for Highly Sensitive, Reliable, Wireless, and Wearable Multifunctional Sensor Applications. American Chemical Society (ACS).
16. Hawy HM, Ali IM. Enhancement the photosensitivity of PVA NFs/Si prepared by electrospinning technique. Optik. 2022;267:169659.
17. Ahmad M, Shahid M, Alanazi YM, Rehman Au, Asif M, Dunnill CW. Lithium ferrite (Li0.5Fe2.5O4): synthesis, structural, morphological and magnetic evaluation for storage devices. Journal of Materials Research and Technology. 2022;18:3386-3395.
18. Goldstein JI, Newbury DE, Michael JR, Ritchie NWM, Scott JHJ, Joy DC. Variable Pressure Scanning Electron Microscopy (VPSEM). Scanning Electron Microscopy and X-Ray Microanalysis: Springer New York; 2017. p. 173-185.
19. Goldstein JI, Newbury DE, Echlin P, Joy DC, Romig AD, Lyman CE, et al. Introduction. Scanning Electron Microscopy and X-Ray Microanalysis: Springer US; 1992. p. 1-19.
20. Elgrishi N, Rountree KJ, McCarthy BD, Rountree ES, Eisenhart TT, Dempsey JL. A Practical Beginner's Guide to Cyclic Voltammetry. J Chem Educ. 2017;95(2):197-206.
21. Abou-Rjeily J, Bezza I, Laziz NA, Autret-Lambert C, Sougrati MT, Ghamouss F. High-rate cyclability and stability of $LiMn_2O_4$ cathode materials for lithium-ion batteries from low-cost natural β−MnO_2. Energy Storage Materials. 2020;26:423-432.
22. Song H, Liu Y, Zhang C, Liu C, Cao G. Mo-doped LiV_3O_8 nanorod-assembled nanosheets as a high performance cathode material for lithium ion batteries. Journal of Materials Chemistry A. 2015;3(7):3547-3558.
23. Wang JL, Li ZH, Yang J, Tang JJ, Yu JJ, Nie WB, et al. Effect of Al-doping on the electrochemical properties of a three-dimensionally porous lithium manganese oxide for lithium-ion batteries. Electrochimica Acta. 2012;75:115-122.
24. Madhu M, Venkateswara Rao A, Mutyala S. La and Ni Co-doping Effect in $LiMn_2O_4$ on Structural and Electrochemical Properties for Lithium-Ion Batteries. J Electron Mater. 2021;50(9):5141-5149.
25. Zhang J, Shen J, Wei C, Tao H, Yue Y. Synthesis and enhanced electrochemical performance of the honeycomb TiO2/$LiMn_2$O4 cathode materials. J Solid State Electrochem. 2016;20(7):2063-2069.
26. Lazanas AC, Prodromidis MI. Electrochemical Impedance Spectroscopy–A Tutorial. ACS Measurement Science Au. 2023;3(3):162-193.
27. Sharifi H, Mosallanejad B, Mohammadzad M, Hosseini-Hosseinabad SM, Ramakrishna S. Cycling performance of $LiFePO_4$/graphite batteries and their degradation mechanism analysis via electrochemical and microscopic techniques. Ionics. 2021;28(1):213-228.
28. Priyono S, Hardiyani S, Syarif N, Subhan A, Suhandi A. Electrochemical performanceof $LiMn_2O_4$ with varying thickness of cathode sheet. Journal of Physics: Conference Series. 2019;1191:012022.